

Naval Research Laboratory

Washington, DC 20375-5320



2

AD-A259 797



NRL/FR/5621--93-9538

Asteroid Detection and Monitoring Using a Satellite-borne Visible Scanner

WILLIAM A. SHAFFER
MARTIN J. McHUGH
DEXTER WANG

*Advanced Concepts Branch
Optical Science Division*

January 15, 1993

DTIC
ELECTE
FEB 2 1993
S c D

93-01805

11/25
11/28

Approved for public release; distribution unlimited.

REPORT DOCUMENTATION PAGE			Form Approved OMB No. 0704-0188
<small>Public reporting burden for this collection of information is estimated to average 1 hour per response, including the time for reviewing instructions, searching existing data sources, gathering and maintaining the data needed, and completing and reviewing the collection of information. Send comments regarding this burden estimate or any other aspect of this collection of information, including suggestions for reducing this burden, to Washington Headquarters Services, Directorate for Information Operations and Reports, 1215 Jefferson Davis Highway, Suite 1204, Arlington, VA 22202-4302, and to the Office of Management and Budget, Paperwork Reduction Project (0704-0188), Washington, DC 20503.</small>			
1. AGENCY USE ONLY (Leave Blank)	2. REPORT DATE January 15, 1993	3. REPORT TYPE AND DATES COVERED	
4. TITLE AND SUBTITLE Asteroid Detection and Monitoring Using a Satellite-borne Visible Scanner		5. FUNDING NUMBERS PE 62111N PN RU11G52	
6. AUTHOR(S) William A. Shaffer, Martin J. McHugh, and Dexter Wang*			
7. PERFORMING ORGANIZATION NAME(S) AND ADDRESS(ES) Naval Research Laboratory Washington, DC 20375-5320		8. PERFORMING ORGANIZATION REPORT NUMBER NRL/FR/5621-93-9538	
9. SPONSORING/MONITORING AGENCY NAME(S) AND ADDRESS(ES) Office of Naval Technology Arlington, VA 22217-5000		10. SPONSORING/MONITORING AGENCY REPORT NUMBER	
11. SUPPLEMENTARY NOTES *SSG, Inc., 150 Bear Hill Road, Waltham, MA 02154			
12a. DISTRIBUTION/AVAILABILITY STATEMENT Approved for public release; distribution unlimited.		12b. DISTRIBUTION CODE	
13. ABSTRACT (Maximum 200 words) A satellite-borne visible scanner is proposed to continuously monitor the celestial sphere for near Earth asteroids. The proposed scanner uses the parallax motion of near Earth objects against a fixed background of distant objects. Image processing techniques will allow the detection of asteroids as small as 50 m in diameter at distances greater than 7×10^6 km. This will give sufficient warning time against Earth intersecting asteroids.			
14. SUBJECT TERMS Asteroids Frame differencing		Visible scanner Parallax	15. NUMBER OF PAGES 12
		Satellite Near-Earth Objects	16. PRICE CODE
17. SECURITY CLASSIFICATION OF REPORT UNCLASSIFIED	18. SECURITY CLASSIFICATION OF THIS PAGE UNCLASSIFIED	19. SECURITY CLASSIFICATION OF ABSTRACT UNCLASSIFIED	20. LIMITATION OF ABSTRACT SAR

CONTENTS

INTRODUCTION.....	1
ASTEROID DETECTION.....	1
Asteroid Detection in the Infrared.....	1
Asteroid Detection in the Visible.....	2
PROPOSED VISIBLE SCANNER.....	5
IMAGE PROCESSING.....	7
CONCLUSIONS.....	7
REFERENCES.....	8

DTIC QUALITY INSPECTED 3

Approved For		
NTIC	22221	<input checked="" type="checkbox"/>
2222 742		<input type="checkbox"/>
Unannounced		<input type="checkbox"/>
Justification		
By		
Distribution/		
Availability Codes		
Avail and/or		
Dist	Special	
A-1		

ASTEROID DETECTION AND MONITORING USING A SATELLITE-BORNE VISIBLE SCANNER

INTRODUCTION

Collisions of planetary bodies with the Earth have played an important role in the geological, biological, and climatological development of the Earth. Asteroid collisions may have had a significant impact on biological evolution as a result of mass extinctions brought on by global climate change [1-3].

Over 200 Near Earth Asteroids (NEAs) have been discovered. The Aten and Apollo class asteroids have Earth-intersecting orbits. NEAs are usually smaller than 5 km in diameter and have short lifetimes compared to the age of the solar system. They are believed to arise from the decay of cometary nuclei or from ejection from the main asteroid belt [4-7].

Asteroid collisions in modern times have demonstrated their destructive power. The 1908 Tunguska meteorite, the 1947 Sikhote-Alin meteorite [8], and the 1945 meteor explosion over the Pacific Ocean all released energies equivalent to small thermonuclear devices. The recent near hit of an asteroid with the Earth (170,000 km) [9] underscores the vulnerability of our planet to sudden devastation.

Based on these concerns, Congress ordered NASA to develop techniques to monitor for potential asteroid collisions. One result of the NASA committee work was the identification of the potential threat posed by asteroids as small as 50 m in diameter. However, objects that small are not reliably detectable using ground-based telescopes because of atmospheric interference as well as manpower considerations. One of the suggestions of the NASA committee was to use a passive detection system in space with DOD derived technologies.

In this report we consider the feasibility of space-based, passive asteroid monitoring using Focal Plane Array (FPA) technology and image processing techniques. In the next section, we compare the detection capabilities of infrared and visible FPAs. Based on this analysis we describe our proposed visible scanner in the third section.

ASTEROID DETECTION

Asteroid Detection in the Infrared

Infrared imagers have long been used to obtain high-resolution data of the Earth's surface [10-12]. Image processing algorithms have been developed to extract faint unresolved moving targets from a temporal sequence of infrared images [13].

The maturity of this technology led us to consider the possibility of using a space-based infrared (IR) scanner to monitor asteroids. We assumed a detector noise equivalent irradiance (NEAI) of 10^{-14} W/cm² and a waveband of 8 to 14 μ m (the region used by Morrison [14]). For an asteroid of radius R and a distance r from the sensor, the irradiance at the aperture in the waveband λ_1 to λ_2 is given by

$$I = \frac{\pi R^2}{r^2} \int_{\lambda_1}^{\lambda_2} (1 - \rho_\lambda) L_\lambda(T) d\lambda \quad , \quad (1)$$

where ρ_λ is the asteroid's reflectivity and $L_\lambda(T)$ is the spectral blackbody radiance at temperature T . Asteroid temperatures typically range from 180 to 280 K with a spectrally averaged temperature of 255 K [15]. The contribution from the background is negligible.

With this in mind, we solve Eq. (1) for the detection range r for the cases $I = \text{NEAI}$ and $3 \times \text{NEAI}$. The results are shown in Table 1 for 50-m and 1-km diameter asteroids. For larger asteroids, warning times are proportionately larger.

Table 1 — IR Detection of 50-m and 1-km Diameter Asteroids.

R (m)	T (K)	$\int L_\lambda$ ($\mu\text{W}/\text{cm}^2\text{sr}$)	r (km) { $I = \text{NEAI}$ }	Warning (hr)	r (km) { $I = 3 \times \text{NEAI}$ }	Warning (hr)
25	180	295	7,400	0.7	4,300	0.4
	255	2,474	21,000	1.9	12,000	1.1
	280	3,967	27,000	2.5	16,000	1.5
500	180	295	150,000	14.	86,000	8.0
	255	2,474	420,000	39.	240,000	22.
	280	3,967	540,000	50.	320,000	30.

Although asteroid detection in the IR is possible, the warning time (assuming an asteroid radial velocity of 3 km/s) associated with small asteroids is not sufficient to deploy countermeasures.

Asteroid Detection in the Visible

While the emitted radiation is concentrated at longwave IR wavelengths, there is also considerable visible light reflected from asteroids. A theoretical comparison of the emitted and reflected radiance of an asteroid is shown in Fig. 1. The efficacy of using visible as opposed to IR depends on the sensitivities achievable in these wavebands.

The irradiance reflected to the sensor by a spherical asteroid in the waveband λ_1 to λ_2 is given by

$$I = \frac{\pi}{4} (\cos \theta + 1) \left(\frac{R_s}{r_s} \right)^2 \left(\frac{R}{r} \right)^2 \int_{\lambda_1}^{\lambda_2} \rho_\lambda L_\lambda(T_s) d\lambda, \quad (2)$$

where

$T_s = 5700$ K is the Sun's effective blackbody temperature,

R_s is the radius of the Sun,

r_s is the distance from the Sun to the asteroid, and

θ is the angle between the Earth and Sun at the asteroid.

The NEAI of a sensor is defined as the signal irradiance that produces a number of carriers N_s equal to the rms fluctuation in the number of carriers ΔN_{rms} :

$$N_s = \Delta N_{rms}. \quad (3)$$

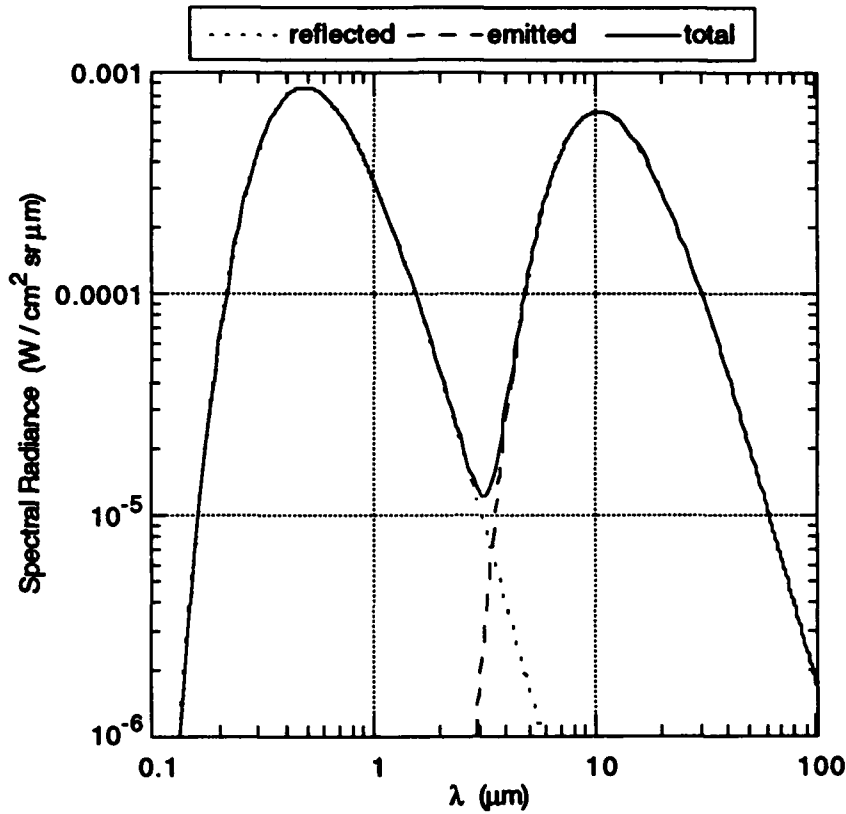


Fig. 1 — Comparison of the emitted and reflected spectral radiance of an asteroid. The asteroid is assumed to be spherical, half lit ($\theta = \pi/2$), at temperature of 280 K and reflectivity of 0.05.

The number of carriers N_s generated by a signal flux ϕ_s incident on a detector of area A_d is given by

$$N_s = \phi_s A_d \tau_i \eta, \quad (4)$$

where τ_i is sample integration time and η is the quantum efficiency of the detector. The noise fluctuations come from two independent sources: detector (dark current) noise and photon noise. The rms fluctuation in the number of carriers from detector noise is

$$\Delta N_d = i_{rms} A_d \tau_i, \quad (5)$$

where i_{rms} is the rms fluctuation in the dark current density. This follows the shot noise expression

$$i_{rms} = \sqrt{2eI\Delta f}, \quad (6)$$

where

e is the electron's charge,
 I is the total dark current through the detector, and
 Δf is the bandwidth of the measurement.

The rms fluctuation in the number of carriers from photon noise is

$$\Delta N_p = \sqrt{(\phi_s + \phi_b) A_d \tau_i \eta} , \quad (7)$$

where ϕ_b is the background photon flux on the detector. To combine two independent random variables, we add their variances:

$$\Delta N_{rms}^2 = \Delta N_d^2 + \Delta N_p^2 . \quad (8)$$

We can now solve Eq. (3) for the noise equivalent photon flux on the detector ϕ_s :

$$\phi_s = \frac{1}{2A_d \tau_i \eta} \left\{ \sqrt{1 + 4[\phi_b A_d \tau_i \eta + (i_{rms} A_d \tau_i)^2]} + 1 \right\} . \quad (9)$$

The NEAI referred to the sensor's aperture is given by

$$NEAI = \frac{A_d}{\tau_o A_o} \frac{hc}{\lambda} \phi_s , \quad (10)$$

where

- h is Planck's constant = 6.63×10^{-34} J s,
- c is the speed of light = 3×10^8 m/s²,
- λ is the wavelength of the observed radiation,
- A_o is the area of the optics, and
- τ_o is the transmission of the optics.

For asteroid detection using image differencing, we require that the minimum observable asteroid radiance is 3 times the noise level or

$$I = NEAI \quad (11)$$

Substituting this in Eq. (2) and solving for r gives

$$r^2 = \frac{\pi}{12} \left(\frac{R_s R}{r_s} \right)^2 \frac{\tau_o A_o}{A_d} \frac{\lambda}{hc} (\cos \theta + 1) \frac{\int \rho_\lambda L_\lambda(T_s) d\lambda}{\phi_s} , \quad (12)$$

where ϕ_s is given by Eq. (9).

If we assume the parameter values listed in Table 2, then Eq. (12) reduces to $r = 2.9 \times 10^8 R$. For a 50-m asteroid, detection is possible at a range of 7×10^6 km. This corresponds to a warning time of 28 days (assuming a relative asteroid velocity of 3 km/s).

Table 2 — Asteroid Detection Parameters

$R_s = 7.0 \times 10^5 \text{ km}$	$A_o = 1134 \text{ cm}^2$
$r_s = 1.5 \times 10^8 \text{ km}$	$A_d = (0.001 \text{ in.})^2$
$\theta = 0$	$\tau_o = 0.7$
$\rho_\lambda = 0.15$	$\eta = 0.9$
$\lambda = 0.75 \text{ mm}$	$i_{rms} = 100 \text{ elec/s}/(0.001 \text{ in.})^2$
$\tau_i = 49 \text{ ms}$	$\phi_b = 3.52 \times 10^7 \text{ photon/cm}^2/\text{s}$

PROPOSED VISIBLE SCANNER

We propose a satellite-based visible scanning instrument that will cover the entire celestial sphere every day with a pixel size of 0.05 mrad. Two linear detector arrays (bars) will produce a pair of images with a 3.2-min time delay. These two images when processed will reveal asteroids as moving objects because of parallax.

The satellite will have an altitude of 770 km (100 min/orbit). The instrument on board the satellite will consist of two 4096 element linear arrays sensitive in the visible wavelength region. Each detector will have instantaneous field of view (IFOV) of 0.05 mrad. The swaths of the arrays will be inclined by 11.49° , corresponding to a 3.2-min delay for this orbital altitude. The entire celestial sphere can be sampled in one day (15 orbits). This is depicted in Fig. 2.

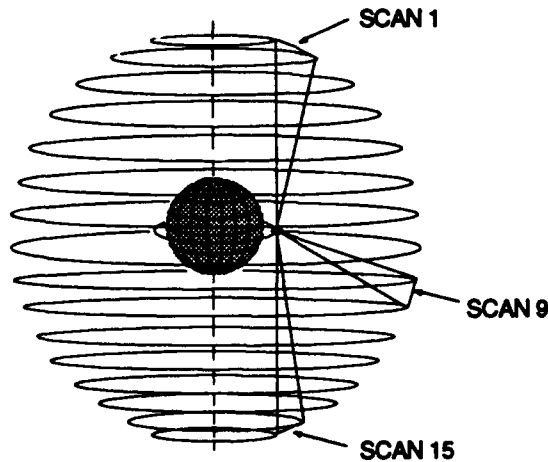


Fig. 2 — Search pattern of the asteroid detection satellite. The detector array sweeps out a 12° swath of the celestial sphere in one orbit. The line of sight is stepped 12° each orbit, so the entire sphere is covered in 15 orbits.

The delay between the images from the two bars will result in parallax motion of near objects as illustrated in Fig. 3. For objects $1.5 \times 10^6 \text{ km}$ from the satellite, the parallax motion between images will be 20 pixels (assuming a 0.05 mrad IFOV). Objects at $3 \times 10^7 \text{ km}$ distance will exhibit parallax motion of approximately 1 pixel. An asteroid with a diameter of 50 m will be detected and tracked with this system at a distance up to $7 \times 10^6 \text{ km}$. Larger asteroids will be detected at correspondingly larger distances, as shown in Fig. 4.

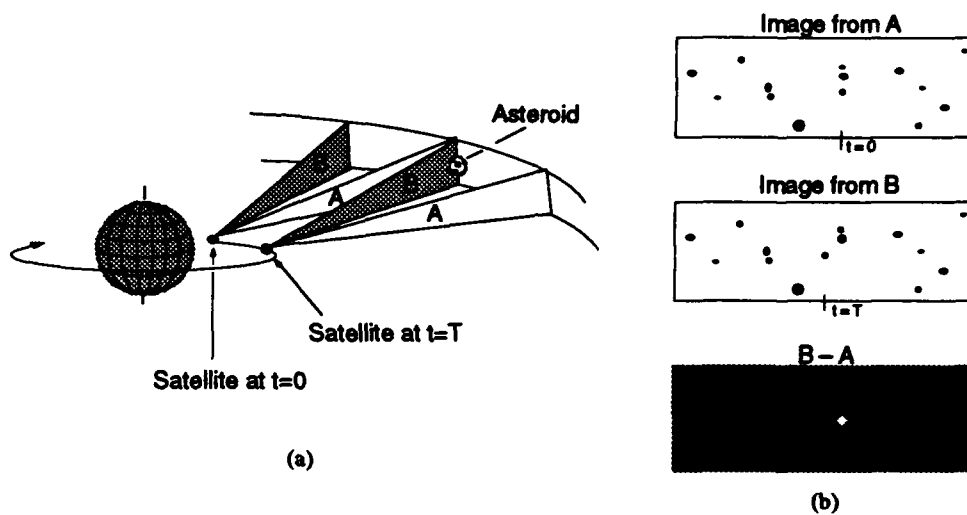


Fig. 3 — Use of parallax to detect near Earth objects. (a) An asteroid is seen at $t = 0$ by detector array A and at time T later by array B. The two arrays see it at different angles (depending on its distance) and hence at a different spot on the star field. (b) The images formed by the scans of the two arrays show the asteroid in different locations in the star field. A frame difference of the images results in a dipole image of the asteroid.

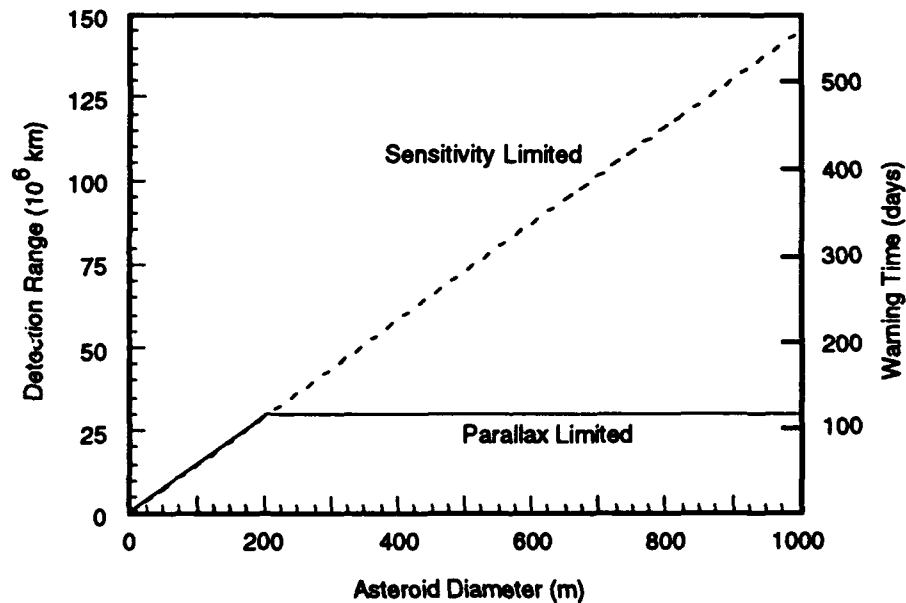


Fig. 4 — Maximum detection range with a visible sensor as a function of asteroid size. The asteroid is assumed fully lit with a reflectivity of 0.15. The cutoff at 3×10^7 km occurs because asteroids more distant than this will not have enough parallax motion to survive the proposed detection algorithm. The dashed line indicates the detection range based on sensitivity alone (Eq. 12).

The dashed line is a plot of Eq. (12) for the parameters listed in Table 2. It represents the range at which the observed asteroid signal exceeds 3 times the noise level of the detector. At this distance, asteroids will appear as unresolved point sources in the scanned image. The solid line in Fig. 4 indicates the range of detectability for an asteroid detected using frame difference signal processing. The maximum value for the range of detectability is determined by the parallax angle between the detector bars. Larger asteroids beyond this maximum range will exhibit subpixel parallax motion that will be canceled in frame differencing. This implies that at the maximum parallax range of 3×10^7 km, the observed signal from asteroids greater than 200 m in diameter will be much greater than the noise level. This could significantly improve change detection algorithms.

Because of the sensitivity of a visible scanner, modifications to the present scheme would allow larger detection ranges and longer warning times. The maximum parallax range in Fig. 4 could be increased by increasing the parallax angle between detector bars. However, significant increases in this angle could require the use of an additional satellite platform. An alternate scheme could involve the use of more computer storage intensive algorithms that compare single images to assumed known star charts. These modifications, however, represent improvements on an experimental concept capable of asteroid detection with sufficient warning time.

IMAGE PROCESSING

NEAs will exhibit parallax motion in the pair of images obtained by this visible scanner. Positive asteroid detection is achieved by differencing the temporal sequence of images. After frame difference signal processing (FDSP), fixed objects will subtract to zero (i.e., below the sensor noise level) in the difference frame. Those exhibiting parallax motion will appear as dipoles (positive-negative pairs).

The first step in an FDSP is image registration and resampling. Image pairs are resampled on a common grid. This requires finding the displacement between them [16,17] and applying some sort of interpolator [18,19]. The resampled images are differenced. Asteroid detection is accomplished by identifying residual dipoles in the difference frame. With good registration and resampling algorithms, residual clutter in the difference frame will be near the sensor noise level. Therefore, asteroids near the sensor noise level will be detected as long as they exhibit sufficient parallax motion.

An important issue in implementing this sensor design is the amount of storage required for an FDSP. If Δt is the time to collect a large enough image to allow differencing and ΔT is the time delay between bars (e.g., 3.2 min), then the buffer size needs to accommodate $N_s(\Delta T + 2\Delta t)$ samples of data, where N_s is the number of samples per minute collected by one bar. The time increment Δt is large enough to allow registration of the partial images.* The first N_s portion of the first image is registered to the second image.

The results from the FDSP are downloaded to a ground station. Further processing on the ground includes classification, orbit tracking (using a time sequence of difference frames), and Earth collision determination and warning.

CONCLUSIONS

Congress has recently called for the investigation of techniques to monitor for potential asteroid encounters. There are unresolved questions regarding the risk associated with asteroids of 50 m to 1 km in diameter. In the previous analysis, we determined that a visible scanner would detect asteroids as small as 50 m in size at ranges over 7×10^6 km. This gives enough warning time for appropriate countermeasures. Infrared detection, suggested by other groups, is possible, but at current sensitivities, the detection ranges would be at least 400 times smaller.

We propose a space-based visible scanner to monitor the entire sky every day. This sensor would see asteroids in the size range of interest (50 m to 1 km and larger) at sufficient ranges. Additionally, the detection of non-Earthbound asteroids this small would give new insight into the distribution of asteroid sizes and orbits and would lead to a better understanding of the nature of the asteroid risk.

* If we assume a linear detector of length 4096 pixels, a dwell time of 50 ms, an image width of 128 samples, and 3 times oversampling, the storage capacity (assuming 2 bytes/sample) required for the two images is 100 Mbytes.

REFERENCES

1. L. W. Alvarez, W. Alvarez, F. Asaro, and H. V. Michel, "Extraterrestrial Cause for the Cretaceous-Tertiary Extinction," *Science* **208**, 1095 (1980).
2. C. C. Swisher III, J. M. Grajales-Nishimura, A. Montanari, S. V. Margolis, P. Claeys, W. Alvarez, P. Renne, E. Cedillo-Pardo, F. Maurrasse, G. H. Curtis, J. Smit, and M. O. McWilliams, "Coeval $^{40}\text{Ar}/^{39}\text{Ar}$ Ages of 65.0 Million Years Ago from Chicxulub Crater Melt Rock and Cretaceous-Tertiary Boundary Tektites," *Science* **257**, 954-958 (1992).
3. P. Claeys, J.-G. Casier, and S. V. Margolis, "Microtektites and Mass Extinctions: Evidence for a Late Devonian Asteroid Impact," *Science* **257**, 1102-1104 (1992).
4. J. Wisdom, "Chaotic Behavior and the Origin of the 3/1 Kirkwood Gap," *Icarus* **56**, 51 (1983).
5. J. Wisdom, "Meteorites May Follow a Chaotic Route to Earth," *Nature* **315**, 731 (1985).
6. G. W. Wetherill, "Where Do the Apollo Objects Come From?" *Icarus* **76**, 1 (1988).
7. R. P. Binzel, S. Xu, S. J. Bus, and E. Bowell, "Origins for the Near-Earth Asteroids," *Science* **257**, 779 (1992).
8. E. L. Krinov, "The Tunguska and Sikhote-Alin Meteorites," in *The Moon, Meteorites and Comets*, B. M. Middlehurst and G. P. Kuiper, eds. (The University of Chicago Press, Chicago, 1963), Ch. 8, pp. 208-234.
9. R. Matthews, "A Rocky Watch for Earthbound Asteroids," *Science* **255**, 1204 (1992).
10. B. A. Buckley and M. L. Burnell, "HiCamp II User's Handbook," Lockheed Report No. LMSC-F044351, Revision A, October 1987.
11. F. D. Palluconi and G. R. Meeks, "Thermal Infrared Multispectral Scanner (TIMS): An Investigator's Guide to TIMS Data," NASA Jet Propulsion Laboratory publication No. JPL 85-32, June 1985.
12. S. Feden and F. Gordon, Jr., "Landsat Satellites," in *Manual of Remote Sensing*, R. N. Caldwell, ed. (American Society of Photogrammetry, Falls Church, VA, 1983).
13. R. L. Lucke, W. A. Shaffer, and R. B. Rhodes, "Computer Simulation of a Space-Based Infrared Surveillance Sensor," NRL Report 9508, Sept. 1992.
14. D. Morrison, "Radiometric Diameters and Albedos of 40 Asteroids," *Astrophysical Journal* **194**, 203 (1974).
15. W. L. Wolfe and G. J. Zissis, eds., *The Infrared Handbook*, Revised Edition (Environmental Research Institute of Michigan, Ann Arbor, 1989), pp. 3-33.
16. W. Shaffer and R. Lucke, "Simultaneous Registration and Nonuniformity Correction of Space-Based IR Images for a Scanning Sensor," Proceedings of the 1992 Meeting of the IRIS Special Group on Targets, Backgrounds and Discrimination, 28-30 January, 1992, Orlando, FL.
17. A. Schaum and M. McHugh, "Analytic Methods of Image Registration: Displacement Estimation and Resampling," NRL Report 9356, Feb. 1991.
18. R. Lucke and A. Stocker, "Filtering Interpolators," NRL Report NRL/FR/6521-92-9505, July 1992.
19. A. Schaum, "Dual Differencing Filtering for Change Detection in Digital Imagery," submitted to *IEEE Image Processing*.